Version of Record: https://www.sciencedirect.com/science/article/pii/S135223102100491X
Manuscript_bff23ab5f3df25c5c31b85c1a0e70a7b

Observations of bay-breeze and ozone events over a marine site during the OWLETS-2 campaign

Vanessa Caicedo*[a,b], Ruben Delgado[a,b], Winston Luke[c], Xinrong Ren[c,d], Paul Kelley[c,d], Phillip R. Stratton[d], Russell R. Dickerson[d], Timothy Berkoff[e], Guillaume Gronoff[e,f]

[a] Joint Center for Earth Systems Technology, Baltimore, Maryland, USA

[b] University of Maryland Baltimore County, Baltimore, Maryland, USA

[c] Air Resources Laboratory, National Oceanic and Atmospheric Administration, College Park, Maryland, USA

[d] University of Maryland, College Park, Maryland, USA

[e] NASA Langley Research Center, Hampton, Virginia, USA

[f] Science Systems and Applications Inc., Hampton, Virginia, USA

*Corresponding author: Vanessa Caicedo (vacaiced@umbc.edu)

Abstract

Land-sea recirculation such as bay and sea-breezes are important local circulations that facilitate pollution events. Measurements over a marine site in the Chesapeake Bay revealed the evolution of two bay-breeze events and associated ozone vertical structure. The horizontal and vertical structure of the bay-breeze was detailed using scanning Doppler wind lidar measurements and a ground-based ozone lidar was used to characterize the vertical distribution of ozone. The two bay-breeze events on 29-30 June 2018 observed during the Ozone Water-Land Environmental Transition Study Phase 2 (OWLETS-2) campaign showed distinct differences in the horizontal and vertical evolution of wind as well as the accompanying vertical structure of ozone. The analysis of the wind circulation showed that the intensity of the offshore flow plays an important role in the initiation time, development, and strength of the bay-breeze on both days. Results showed increased surface ozone concentrations during times of relatively low or decreasing bay-breeze height and weak upwards vertical motion. Upwards vertical motions were significantly enhanced on 30 June 2018 and presented with a decrease in surface ozone concentrations, yet enhanced ozone values were lofted above the surface near the lofted offshore flow. This study shows that both the vertical structure and evolution of pollutants can be impacted by the bay-breeze events through dilution and transport.

Keywords: Land/sea-breeze, Coastal air quality, Ozone pollution, Boundary layer structure

1. Introduction

Bay, sea, or lake breezes are important local meteorological mechanisms that can impact the transport, dispersion, and vertical distribution of pollutants near coastal regions. Coastal regions often experience poor air quality during breeze events as meteorological conditions allowing the formation of local circulations are also conductive of ozone production and ozone precursor accumulation (Banta et al., 2005). For instance, the development of the bay-breeze can create a convergence zone between onshore and offshore flows, developing a region of calm winds that can enable the accumulation of pollutants over emission sources. Air quality can also be impacted by local circulations through recirculated air masses during the bay and the land breeze flows. These recirculated air masses will have physical and chemical properties that originated over land that will be exposed to new marine environments and vice versa. For example, previous studies have shown that the nighttime land breeze can transport ozone over water where it may not be efficiently removed. This can be transported back onshore with the bay-breeze, contributing to daytime ozone concentrations (Banta et al., 2005; Darby, 2005).

Land-water circulations are formed due to differences in the specific heat of land and water bodies and can generate complex air flows. The land-sea circulation for instance, is created with increased surface heating during daytime which will warm air over land surfaces faster than the air over water bodies. The warm air will rise, permitting the relatively cooler marine air to move onshore. This air is then warmed and rises, returning offshore air above the cool onshore air and creating a lofted return flow to close the circulation (Stull, 1988; Tijm et al., 1999). After sunset, the reverse happens, as air over land will cool rapidly with decreased surface heating, while the warmer air over water will rise and allow for the cool land breeze to move offshore. Land-water circulations have been studied for many years as the bay, sea, or lake breeze can play

an important role in near-coastal climates (Pearce 1995 Philandras et al., 1999; Van der Molen et al., 2006), air pollution (Banta et al., 2005; Darby, 2005; Darby et al., 2007), severe weather (Sills et al., 2002; King et al. 2003; Vemado et al., 2016), and convective initiation (Kingsmill 1995; Azorin-Moline et al. 2009).

Understanding the complex interactions of the bay, sea, or lake breeze and its impacts on the vertical distribution of pollutants is vital in coastal regions. With the increasing availability of observational and numerical model technology, the horizontal and vertical development of the bay-breeze has been observed in many highly populated cities (Banta et al., 2005, Banta et al, 1993, Darby et al., 2002; Loughner et al., 2014; Zen et al., 2017, Curry et al., 2017; Caicedo et al., 2019). However, measurements during these complex circulations are limited, particularly over water bodies. Numerical models are also challenged in this dynamic environment as small variations in timing and strength of the bay breeze can impact pollutant concentration and distribution (Caicedo et al., 2019). For example, the Baltimore-Washington region (impacted by local emissions sources from vehicles, power plants, and ships) has seen associations between high pollution events and bay-breeze circulations. During these complex local circulations, observations and model simulations have presented with high pollutant concentrations over the Chesapeake Bay (Zhang et al., 2009; Zhang et al., 2011; Goldberg et al., 2014; Stauffer and Thompson, 2015; Mazzuca et al., 2019). However, as Loughner et al. (2011; 2014) highlighted, the complexities in these events showed that strength, location, and direction of the bay-breeze had varying effects in the horizontal and vertical distribution of pollutants. Further, the role of the bay-breeze circulation on boundary layer venting over water bodies remains unclear.

More recent campaigns have sought to increase our understanding of local circulations and associated pollution by focusing on contrasting measurements over continental and marine

environments. The 2017 Lake Michigan Ozone Study (LMOS) (Abdi-Oskouei et al., 2020; Vermeuel et al., 2019) and 2018 Long Island Sound Tropospheric Ozone Study (LISTOS) sought to understand elevated ozone along the coast of Lake Michigan and Long Island Sound, respectively. Similarly, the Ozone Water-Land Environmental Transition Study (OWLETS-1 and OWLETS-2) was designed to observe ozone and meteorological gradients over continental and coastal regions in the Chesapeake Bay area (Sullivan et al., 2018; Dacic et al., 2020). We use the rare marine profiling data set from the OWLETS-2 campaign to better understand the bay-breeze dynamics and its role in the vertical redistribution of pollutants over water bodies.

This study presents the evolution of two bay-breeze events and associated vertical evolution of ozone in a marine environment using observations within the Chesapeake Bay. The selected cases on 29 and 30 June 2018 present with both high surface ozone concentrations (10-minute peak averaged 94 ppbv at 16:20 LST and 104 ppbv at 13:10 LST, respectively) and local re-circulations of the Chesapeake Bay and land breeze. Using various Doppler wind lidar scanning techniques and derivations, the development of two distinctively different bay-breeze events were detailed and connected to the observed surface and vertical distribution of ozone within the Chesapeake Bay (HMI) site. Data, instrumentation, and methods are described in Section 2, and the bay-breeze case studied are presented in Section 3. Section 4 presents discussion and conclusions for this study.

2. Data and Methods

The Ozone Water-Land Environmental Transition Study (OWLETS) sought to improve the understanding of the physical and chemical interactions of water–land transitions in the Chesapeake Bay. While initial measurements were conducted in the Tidewater region of

Southeastern Virginia in 2017 (OWLETS-1), the summer of 2018 was focused on the Baltimore-Washington region (OWLETS-2) from 6 June 2018 to 6 July 2018. OWLETS-2 super sites were chosen to observe differences between inland and marine gradients. Here we focus on the Hart Miller Island (HMI) site for continuous marine measurements (Figure 1). The research site is located within the Chesapeake Bay (39.2449 °N, -76.3583 °E, 0 m ASL) approximately 20 km east of downtown Baltimore, MD. The site combined profiling remote sensing instrumentation, chemical and meteorological surface analyzers, and sounding systems. HMI has no emission sources near or on the island, but can be affected by transport from Baltimore, MD under westerly and northwesterly offshore flow. The Baltimore area is one of the major metropolitan areas in the US Mid-Atlantic region and hosts a combination of utility plants, industrial compounds, and heavy vehicle traffic. Under the land and bay circulation, offshore flow can containing various source of emission from the Baltimore-Washington area which can be transported over the Chesapeake Bay contributing to high pollutant values within the Bay (Loughner et al. 2011; 2014; Zhang et al. 2011; Stauffer et al. 2015).

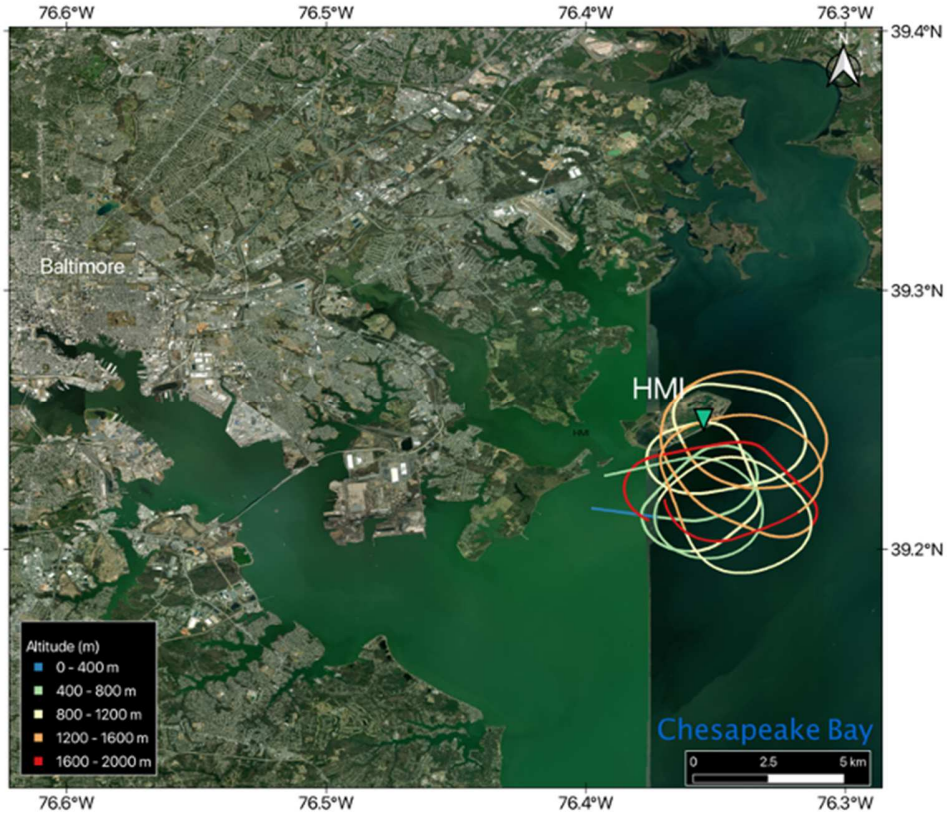

Figure 1. Image of the marine site Hart Miller Island (HMI) in the upper Chesapeake Bay. Green triangle denotes the location of instrumentation deployment. Aircraft flight tracks used in this study are also displayed.

2.1 Instrumentation

HMI measurements used in this study include a Doppler wind lidar, a tropospheric ozone lidar, surface chemistry, and meteorological measurements as well as ozonesonde balloon launches. The Doppler wind lidar (DWL) deployed at the site (at ground level) was the Leosphere WINDCUBE 200s. The lidar scanning approach consisted of a conical scanning pattern at five elevations (0º, 5º, 10º, 35º, 70º) for approximately 10 minutes in total for each scanning pattern, followed by an 8-minute vertical stare. Conical scans detail both the horizontal and vertical development of the bay-breeze while the vertical stares are used for insight into

97 vertical motions. Low-elevation-angles (5º and 10º) in particular, are key for capturing the
98 shallow bay-breeze horizontal variability of the winds, particularly in low altitudes.

99 The NASA LaRC Mobile Ozone Lidar (LMOL; De Young et al. 2017; Farris et al. 2018,
100 Gronoff et al. 2019) deployed on HMI is a ground-based tropospheric ozone lidar that uses a
101 dual-wavelength, ultra-violet pulsed laser which allows for the calculation of ozone vertical
102 profiles by atmospheric differential absorption (Leblanc et al., 2016; 2018) at 5-minute temporal
103 resolution and vertical resolution from approximately 50 m to 1 km. Here, we use reported data
104 from ~104 m above ground level at a 10-minute temporal and with varying vertical resolutions to
105 maintain signal-to-noise below 10%. Surface measurements of ozone and meteorological
106 parameters (wind speed, direction, temperature, relative humidity, and pressure) were also
107 available at HMI; here we use 10-minute averages of surface measurements for comparison to
108 10-minute ozone lidar measurements.

109 The University of Maryland Cessna 402B research aircraft was deployed during the
110 OWLETS-2 to conduct flights over Baltimore and its surrounding areas and is used here to
111 support DWL and ozone lidar measurements. A detailed description of the aircraft
112 instrumentation can be found in Ren et al. (2018). The aircraft was equipped with a modified
113 Thermal Electron Model 49C ozone analyzer based on UV absorption. Temperature, pressure
114 and relative humidity were measured by a Vaisala combined T/P/RH transmitter (Model
115 PTU300). Horizontal wind speed and wind direction were calculated based on the measurements
116 of true airspeed, ground speed, and ground track angle by the aircraft Garmin G600 system and
117 true heading by a Hemisphere differential GPS (Model VS330) (Conley et al., 2014). Vertical
118 spirals over the HMI site used in this study are shown in Figure 1. Although the aircraft
119 performed 4 vertical spirals on June 20-30, we limit aircraft data to the spirals reaching the

lowest altitudes while still remaining over water resulting in the first measurements available at 431 m and 304 m on 29 June and 30 June, respectively.

The period from 29 to 30 June 2018 was selected for this study as both enhanced surface ozone and bay-breeze circulations were observed. Additionally, these days were classified as intensive days during the campaign period which consisted of rigorous and concentrated measurement efforts allowing for continuous ozone lidar, Doppler wind lidar, and twice daily radiosonde launches.

2.2 Bay-breeze Identification

The bay-breeze occurrences during the field campaign were identified following Sills et al. (2011) and Mariani et al. (2017), using both DWL and surface measurements. The criteria used to identify bay-breeze periods are: 1) a daytime wind direction change from offshore to onshore flow of more than 100º, 2) a decrease of radial velocities to less than 4 m/s followed by an increase in radial velocities (at least double) within the onshore flow, and 3) an increase in dew point temperature (>1 ºC). Due to the irregular shoreline of the area (Figure 1), flow from the W to N directions are indicative of offshore flow while flows from E to S directions (perpendicular to mainland coastlines and HMI western shore) are indicative of onshore flow.

During the onset of the bay-breeze, warm air over land will rise permitting the relatively cooler marine air to move onshore. This elevated warm air will return offshore above the onshore bay-breeze flow, forming a lofted return flow and completing the local circulation. Under these conditions, the Chesapeake Bay will experience opposing flows of onshore flow near the surface and offshore flow above. To study the vertical evolution of the bay-breeze flow over the Chesapeake Bay, a combination of individual conical scans at elevation angles 5º, 10º, 35º, and 70º from ~45º to 270º azimuth (0º represents North) were analyzed to determine the vertical

143 extent of the bay-breeze flow at the boundary between offshore and onshore flow. This subset
144 azimuth range was selected to easily identify flow towards the lidar indicative of onshore flow. If
145 opposing flows (near-surface onshore flow and offshore flow above) were detected, the height
146 where onshore flow transitioned to offshore flow was calculated. All transition heights were then
147 averaged throughout the study period, and hereafter referred to as the bay-breeze height (BBH).
148 Radiosonde launches were used to validate the BBH and identify the thermodynamically derived
149 planetary boundary layer (PBL). Ozonesonde launches were performed twice daily at ~12:00 and
150 15:00 Local Standard Time (LST = UTC-5 hours) for both case study days. The radiosonde
151 derived PBL height was determined following Heffter (1980) and Snyder and Strawbridge
152 (2004) for stable layers. The PBL heights derived from the two radiosondes at 12:11 and 15:03
153 LST on 29 June (12:14 LST and 15:02 LST on 30 June) were identified to be 458 m and 602 m
154 (500 m and 574 m), respectively, while DWL BBHs at launch time were calculated to be 408±41
155 m and 584±106 m (462±25 m and 606±25 m), respectively. Radiosondes remained over HMI at
156 the time of the derived PBL height and within 0.5 km the DWL. Agreement between DWL
157 BBHs and radiosondes indicate that the BBH is representative of the marine thermodynamic
158 boundary layer height. Vertical velocity variance measurements are possible with a DWL during
159 the vertical stares at high temporal resolution (Tucker et al., 2009; Bonin et al., 2018). Here, we
160 characterize the turbulence intensity using the variance of the vertical velocity over the 10-
161 minute periods and 100 m in the vertical (Hogan et al., 2009; Barlow et al., 2011) for
162 understanding bay-breeze dynamics associated with vertical distribution of ozone.
163
164 **3. Case study of 29 June and 30 June 2018 bay-breeze events**
165 *3.1 Meteorological conditions*

The meteorological pattern (Figure 2) during the case study consisted of a low-pressure system over the Northeastern United States (New England region), and its associated high-pressure system centered over the inner US Midwest moving east towards the US East Coast. The high-pressure system remained mainly west of the study region on 29 June 2018 (Figure 2a) and passed over the region on 30 June 2018 (Figure 2b). Over the two case study days, the pressure increased from 1016 to 1020 hPa with the proximity of the high-pressure center to the study area. The center of a high-pressure system typically displays increasing temperatures, low cloud cover, and calm winds known to facilitate the formation of a bay-breeze, boost photochemistry production, and allows for the buildup of pollutants under calm conditions.

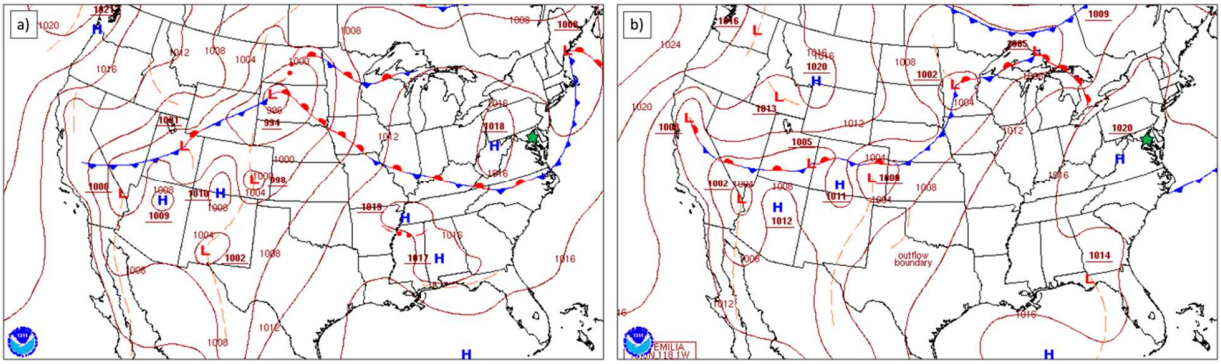

Figure 2. Surface analyses showing a high-pressure system west of study area (green star) on June 29, 2018 01:00 LST (a) and moving towards study area on June 30, 2018 01:00 LST (b). Data from the Hydrometeorological Prediction Center of the National Centers for Environmental Prediction http://www.wpc.ncep.noaa.gov/dailywxmap/

3.2 Bay-breeze DWL observations

The DWL mean wind speed and direction is used to capture the transition from early morning offshore to onshore flow, maturation of the bay-breeze during the daytime, and reversal to offshore flow in the evening on both cases study days (Figure 3). With the center of the high-pressure system west of the study region (Figure 2a), 29 June 2018 presents offshore flow at an average of ~3 m/s near the surface (from 00:00 to 05:00 LST) with higher winds up to ~15 m/s at higher altitudes of ~50 m-850 m (Figure 3a). In the morning (~10:00 LST), winds are calm and

188 the transition to onshore flow begins with offshore flow above the bay-breeze flow. By ~21:30
189 LST surface winds return to offshore direction. As the high-pressure system moves over the
190 study area (Figure 2b), initial conditions on 30 June presents calmer winds at ~1 m/s from
191 ~00:00 - 05:00 LST (Figure 3b). Calm winds early in the morning (04:00 - 11:00 LST) allow for
192 an early onset of the bay-breeze and the development into a strong bay-breeze with wind speeds
193 of ~5 m/s in the afternoon. Wind flows transition back to offshore again by ~21:00 - 22:00 LST.
194 In general, 29 June presented stronger winds both near the surface and within the lofted offshore
195 flow, and a later development of the bay-breeze than that of 30 June. Aircraft measurements
196 support DWL data and closely follow resultant winds over the bay (Figure 3 right panels).

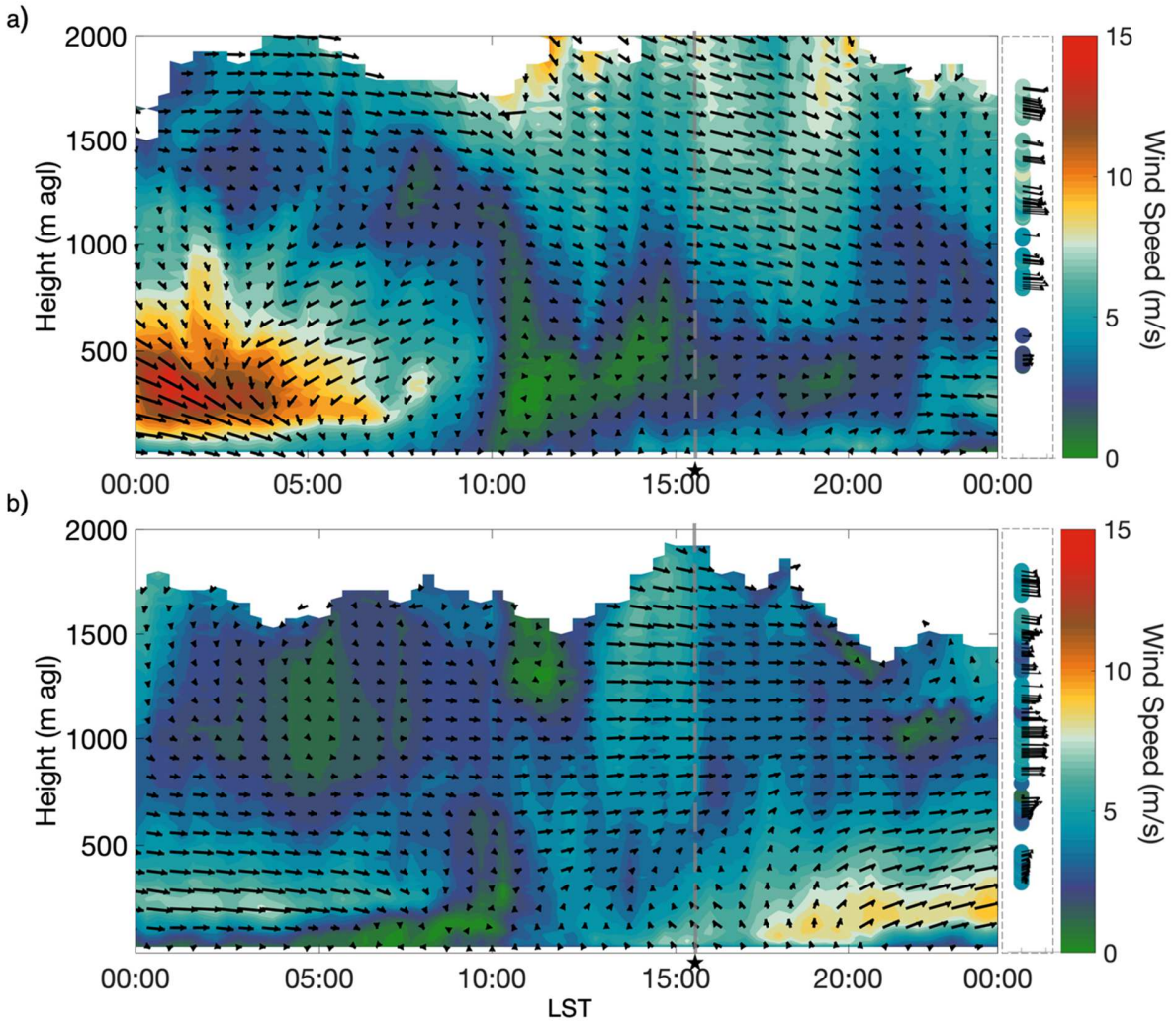

Figure 3. Doppler wind lidar mean wind speed and direction calculated from conical scans during (a) 29 June 2018 and (b) 30 June 2018. Circular markers at the right of each image represent aircraft vertical profiles of winds at approximately 15:38 LST and 15:35 LST on June 29, 2018 (a) and June 30, 2018 (b), respectively (time of aircraft measurements are indicated by grey dashed lined and black star).

During large-scale offshore flow, it is difficult to differentiate between the re-circulation's offshore return flow or the persistent large-scale offshore flow as both present similar wind directions. An increase in wind speed can be indicative of the synoptic and the return flows merging in a single layer. Only 29 June presents with an increase in offshore flow wind speeds while offshore wind speeds during 30 June remain relatively low (Figure 3). Here

209 we refer to an offshore flow above the bay-breeze as a lofted offshore flow likely including the
210 lofted return flow on 29 June and only the large-scale offshore flow on 30 June.

211 DWL radial velocities for conical scans for entire azimuth range (note that scans begin in
212 the North direction = 0 ° azimuth) at 5° (Figure 4) and 35° (Figure 5) above the horizon are
213 presented for both case study days to detail the horizontal and vertical evolution of bay-breeze
214 wind flows over the marine site. The 5° scans allow for the monitoring of shallow flows (up to
215 ~250 m a.g.l.) while the 35° scans can penetrate to higher altitudes (up to ~2100 m a.g.l.) thus
216 providing more information about the winds higher above the ground than the 5° plots. Figures 4
217 and 5 show the DWL radial velocity for from 29 June (a-d) 09:00 LST to 30 June (e-j) 11:15
218 LST to highlight the development of the bay-breeze. Negative velocities shown in green and blue
219 denote flow toward the lidar, while positive velocities shown in yellow and red indicate flow
220 away from the lidar (located at the center of each plot). The height of the lidar beam in relation to
221 the lidar (cyan values) increases with horizontal distance away from the lidar (white values) due
222 to the elevation angle. The height of the lidar beam is important, particularly for the shallow bay-
223 breeze as changes in wind flow away from the lidar can be due to its penetration through various
224 vertical layers or horizontal variability.
225

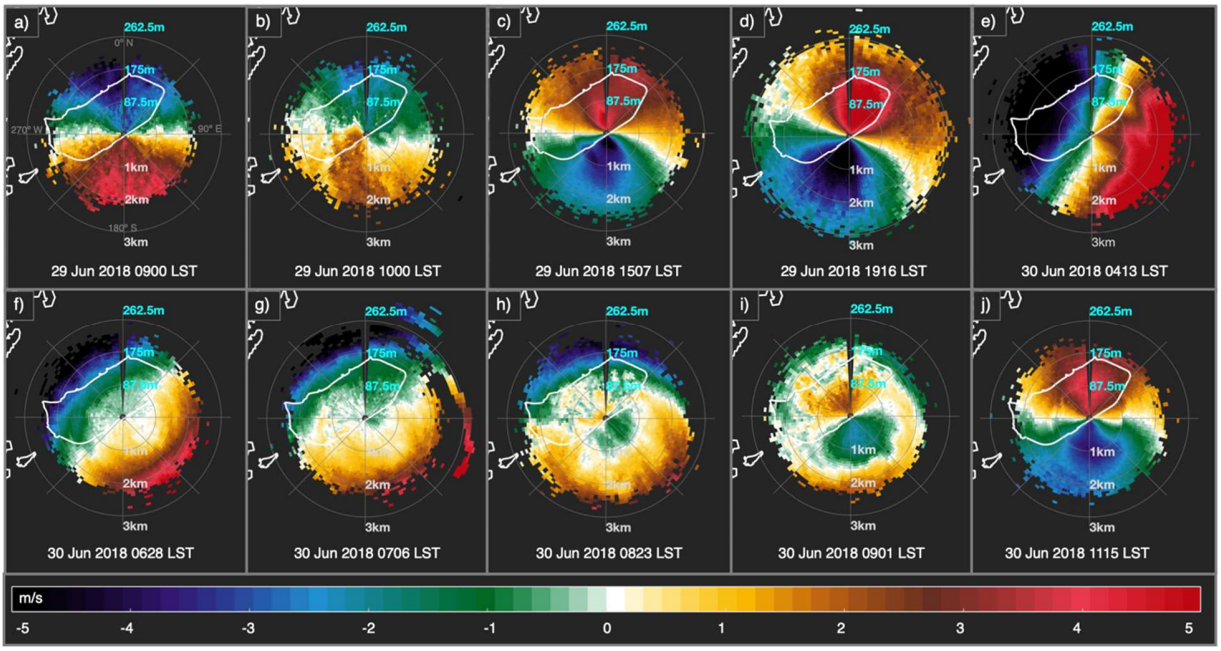

Figure 4. Doppler lidar radial velocity (units: m/s) from five-degree elevation angle showing the evolution of wind flows over the Chesapeake Bay on June 29 (a-d) and June 30 (e-j). Shorelines are displayed in white beneath the lidar measurements. White distance labels indicate the horizontal range from the lidar while cyan values indicate the corresponding vertical height due to the elevation angle. Green and blue indicate flow toward the lidar; yellow and red indicate flow away from the lidar.

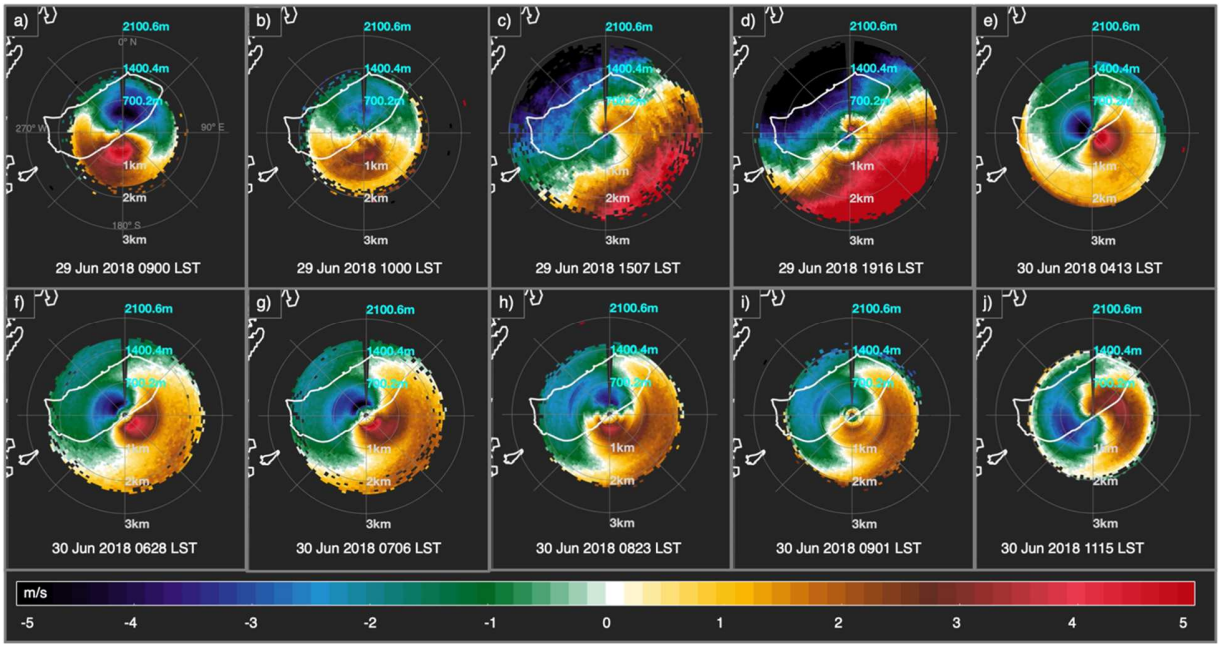

Figure 5. As in Fig. 4 except with a 35° the elevation angle. Note that green and blue indicate flow toward the lidar; yellow and red indicate flow away from the lidar.

Figures 4a and 5a measured on 29 June at 09:00 LST show radial velocities of strong offshore flow from the north through all altitude ranges. Figure 4b at 10:00 LST is the first to display a small region of onshore flow southeast of the lidar (green/blue area within a ~500m horizontal range from the lidar at ~130 ° azimuth) revealing the newly developed bay-breeze with average wind speeds of ~2.1 m/s (sunrise was at approximately 04:40 LST on both days) along with a weakened offshore flow of ~1 m/s allowing for the formation of the bay-breeze. The bay-breeze on 29 June is first detected at ~10:00 LST and continued to show strengthening in Figure 4c (15:07 LST) showing the mature bay-breeze flow reaching the full horizontal and vertical range extension of the 5º scans. The bay-breeze reaches its peak at approximately 14:50 LST at a height of 584 ± 106 m. Figure 5c using 35º elevation angles, reveals the onshore flow detected within the ranges closest to the lidar (green/blue area within ~1000m horizontal range from the lidar from ~130-200º azimuth) but are beyond the range of the 5º scans. The lofted offshore flow (measurements farther away from the lidar) had strengthened to wind speeds of ~5.5 m/s. By 19:16 LST (Figure 4d) scans show the bay-breeze flow with increased windspeeds rotating slightly clockwise, likely due to irregular shoreline variations, synoptic-scale flow variations, and the Coriolis force (Mariani et al., 2017). Figure 5d, reveals a decrease in the bay-breeze horizontal and vertical extent compared to Figure 5c in the measurements closest to the lidar which is confirmed by the decrease in BBH from ~15:00 – 19:00 LST in Figure 6a. The bay-breeze onshore flow is no longer detected, and winds transition back to offshore flow at approximately 21:00 LST on 29 Jun.

NW winds continue throughout the nighttime of 30 June (Figures 4e and 5e). Low elevation scans at 5º show a significant weakening of near-surface winds at 06:30 LST (Figure 4f white areas in ~135 ° azimuth) within ~1 km from the lidar. This weakening is significantly more

prominent than that observed on 29 June. Offshore flow in higher altitudes (Figure 5f) was also weaker than that seen before the onset of the bay-breeze on the previous day. As the bay-breeze develops, a prominent onshore flow is discernable at 07:06 LST (Figure 4g green/blue area ~90-140º azimuth)) close to the surface but not detectable in higher elevation scans in Figure 5g. The vertical and horizontal growth of the bay-breeze is clearly observed in Figures 4f-4i with the bay-breeze centered offshore extending horizontally creating an increasing area of onshore flow (green/blue flow towards lidar) in distances closest to the lidar. Figure 4i displays the bay-breeze flow up to ~1.5 km in horizontal diameter with an average wind speed of ~1.5 m/s. The bay-breeze strengthens and continues to overpower the offshore. By 11:00 LST (Figure 4j) the mature bay-breeze reaches wind speeds of ~4 m/s and extending >2 km horizontally reaching the limit of the DWL range. Offshore flow (Figure 5f-5j) on this day does not increase in speed as that of June 29, as is weaker than that observed in the previous day with speeds of ~3 m/s. The initial weakening of the offshore flow favors the early formation of the bay-breeze, along with a weak offshore flow which allows for the strong development of the bay-breeze on 30 June. In comparison to the previous day, an overall stronger offshore flow (Fig. 5a-b) increasing in strength (Fig. 5c-d), likely limited the horizontal and vertical progression of the bay-breeze on 29 June. With weaker opposing offshore flow on 30 June, the BBH reaches ~881 ± 74 m at 16:24 LST.

Radial velocities during the DWL vertical stares are depicted in Figures 6a and 6c with flow downwards toward the lidar in negative velocities (blue) and upwards away from the lidar in positive velocities (red) for days 29 and 30 respectively. Using the methodology described in Section 2, the depth of the bay-breeze height (BBH) can be monitored and is displayed as the black (white) line in Figure 6a and 6c (Figure 6b and 6d). Vertical velocities on 29 June (Figure

6a) show an increase in vertical velocities at ~9:00 – 10:00 LST indicative of the bay-breeze front, followed by a decrease in vertical motion within the onshore flow as is expected due to the largely horizontal motion of the bay-breeze in addition to relatively lower generation of thermals over water than over land (Mariani et al., 2017). Enhanced vertical velocities are displayed in the lofted offshore flow above the bay-breeze as the embedded characteristics of the offshore flow will advect the land generated thermals offshore above the bay-breeze flow. Figure 6b supports vertical radial velocities and show the highest turbulent intensities within the lofted offshore flow.

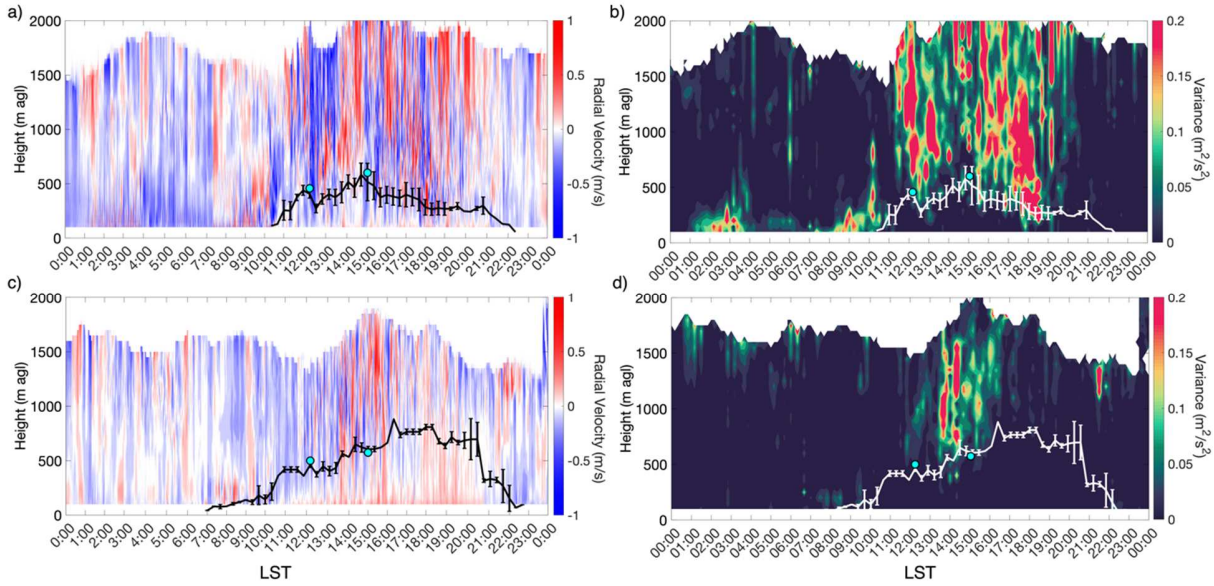

Figure 6. DWL vertical radial velocity (left panel) and vertical velocity variance (right panel) for 29 June (a,b) and 30 June (c,d). Bay-breeze flow height is displayed as the black (left panel) and white (right panel) lines. Radiosonde PBL heights are displayed as the cyan circles. Note that times when the DWL was performing conical scans were not included in the figures.

On 29 June, a decrease in the BBH (Figure 6b at ~17:30-18:30 LST) is observed in conjunction with enhanced turbulent motion adjacent to the calculated BBH which may be suggestive of entrainment of air in the bay-breeze and lofted offshore flows. A strong thermal lofted offshore flow subsiding over water may limit the growth of the bay-breeze. Both layer

303 entrainment and subsidence can be important mechanisms in air pollution as entrainment from
304 above wind flows can change pollutant concentrations and a decrease in the BBH could impact
305 the surface concentrations of pollutants through a reduction of dilution volume.

306 Different than 29 June and previous case studies presented in (Curry et al., 2017; Mariani
307 et al., 2017), the expected reduction in vertical motions is not observed on 30 June. Instead, a
308 clear increase in the upwards motion values is shown within the onshore flow (Figure 6c) that
309 was not seen in the previous day. Bay-breeze is typically associated with a lower thermal
310 generation, yet vertical velocities suggest that a strong bay-breeze can experience larger
311 thermals. The vertical variance (Fig. 6d) supports that the bay-breeze on 30 June developed
312 strong horizontal and vertical flow with a less turbulent opposing flow.

313

314 *3.3 Ozone observations*

315 The dynamics of the bay-breeze can modulate the transport of trace gases, including
316 ozone, as well as its vertical and horizontal distribution. For this reason, the NASA Langley
317 mobile ozone lidar (LMOL) was deployed at HMI in order to closely monitor the temporal and
318 vertical evolution of ozone. LMOL began measurements at approximately 08:00 LST on 29 June
319 2018 (Figure 7a). Ozone concentrations of about ~60 ppbv from ~08:00-10:00 LST are lofted
320 above the marine site within the residual layer from about 200 m to 1500 m with lower
321 concentration of ~50 ppbv near the surface. After sunrise, ozone concentrations both near the
322 surface and above begin to increase, reaching the highest surface concentrations of 93.8 ppbv
323 (10-minute average) at 16:20 LST. The vertical distribution of ozone on 29 June (Figure 7a) is
324 mostly contained within the BBH due to the thermodynamic capping of at the PBL height.

Above the BBH, the lofted offshore flow contains values of ozone ~64 ppbv likely advected from inland sources offshore towards the HMI site.

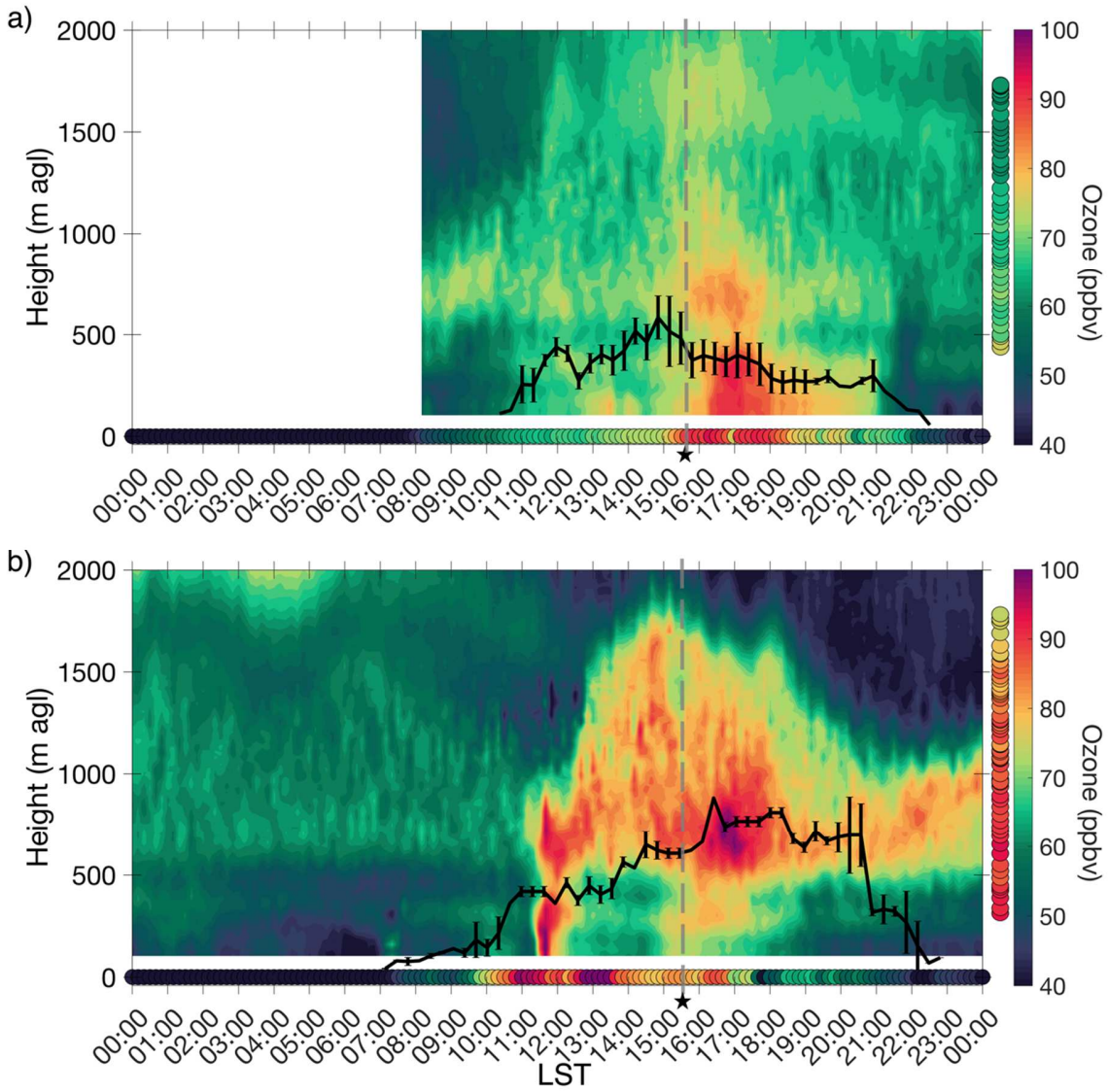

Figure 7. HMI ozone lidar (LMOL) measurements for (a) 29 June 2018 and (b) 30 June 2018. Circular markers at the bottom of each image represent 10-minute surface ozone concentrations. Circular markers at the right of each image represent aircraft vertical profiles of ozone at approximately 15:38 LST and 15:35 LST on June 29, 2018 (a) and June 30, 2018 (b), respectively (time of aircraft measurements are indicated by grey dashed lined and black star). Black lines follow the BBH. Note that no ozone lidar measurements are available before 08:00 LST on 29 June 2018.

A period of enhanced ozone is observed from about 16:00 to 18:00 LST with surface concentrations averaging ~89.4 ppbv and lidar measurements showing ozone well-mixed within the BBH. Concurrently, a small BBH decrease from ~ 500 m to 400 m is observed. It is likely that the reduced dilution volume of the BBH could have contributed to the enhanced surface ozone values, however, peak ozone photochemistry and precursor emission sources cannot be neglected particularly boat activity in the Chesapeake Bay. Aircraft profiles at 15:38 LST do not capture the enhancement in surface ozone concentrations due to the first aircraft measurement over water at 431m but does capture the lower ozone concentrations above the BBH supporting the capping of pollutants at the BBH.

Previous studies have observed consecutive days of local re-circulations can lead to an accumulation of pollutants facilitated by the re-circulation of airmasses. Ozone concentrations on 30 June are overall higher than those on the previous day with the highest surface ozone measured from 11:00 to 14:00 LST with a maximum of 104 ppbv at 13:10 LST. These high ozone values are observed during the early development of the bay-breeze when the BBH remains below 600 m. A lower BBH and a lack of vertical motion create the ideal conditions for high ozone concentrations. These high surface values are higher than those observed in the ozone lidar. Although within the 10% ozone lidar uncertainty, this is likely due to the first available ozone lidar measurements which may not capture near-surface ozone at lower altitudes. After ~14:00 LST, surface ozone decreases along with an increase in upwards motion (Figure 6c). Ozone lidar profiles reveal that ozone is no longer concentrated near the surface instead, high values are lofted above the bay-breeze flow within the offshore flow. As vertical motion increases and surface ozone values decrease, it is likely that the larger upwards motion assisted in the reduction of surface ozone and in maintaining ozone lofted above the surface. An area of

359 high ozone (~100 ppbv) is seen from 16:00-18:00 LST at the BBH boundary at the time when an
360 enhanced vertical variance is also observed (Figure 6d) possibly pointing to entrainment between
361 lofted offshore flow and bay-breeze flow. Aircraft measurements at 15:35 LST capture the
362 enhanced ozone concentrations through the entire vertical spiral and falls within 10% uncertainty
363 when compared to the ozone lidar measurements. Generally, 30 June presented a strong vertical
364 development of the bay-breeze which was coincident with lofted ozone concentrations and lower
365 surface values. As such, the strength of the bay-breeze on this day played a critical role in the
366 vertical distribution of ozone. The aircraft measurements on both days follow the ozone lidar
367 measurements closely. Figure 1 shows the aircraft trajectory for the profiles displayed in Figure
368 6 covering a larger area of the Bay in comparison to the ozone lidar therefore, some of the
369 differences in ozone concentrations are likely due to the spatial area covered by the two
370 platforms.
371
372 **4. Discussion and Conclusions**
373 The profiling systems (Doppler wind lidar and ozone lidar) deployed at the Hart Miller
374 Island site during the OWLETS-2 campaign allowed for the unique monitoring of Chesapeake
375 Bay-breeze dynamics and ozone vertical distribution over a water body. Coastal regions are
376 subject to pollution events often associated with the land and bay-breeze local circulations.
377 Although previous measurement campaigns have observed enhanced ozone over the Chesapeake
378 Bay, these measurements are often limited per event, located at inland sites, and do not offer
379 insights into the bay-breeze vertical dynamics. Hence, the complex interactions between local
380 circulations and impacts on pollutant dilution and distribution over marine environments has not
381 been well observed. Marine air quality is often overlooked as terrestrial air quality will impact a

larger population. Marine environments have faster photolysis rates, slower deposition velocities, and pollution sources from recreational, fishing, and import/transport industry vehicles that can impact recreational activities and inhabitants of coastal areas when bay-breeze dynamics are unfavorable for the diffusion of pollutants.

Local re-circulations due to water-land breezes present the ideal conditions for air quality events as the warm, clear-sky, and calm winds conditions are conductive for increased photochemistry and pollutant accumulation. Further, local re-circulations have been observed to recycle pollutants during consecutive events (Banta et al., 2005; Darby et al., 2005; Loughner et al., 2014; Caicedo et al., 2019). In these cases, onshore daytime accumulation of pollutants during calm conditions during the bay-breeze can be transported offshore during the nighttime land-breeze. These pollutants can then return onshore with the next day's bay-breeze and contribute to enhanced daytime pollutant concentrations. In addition to the recycling of air masses and its embedded pollutants, the role of entrainment during local re-circulations is not well understood. This includes the role of residual layer ozone and possible entrainment into the developing daytime bay-breeze, augmenting surface concentrations. Similarly, the offshore lofted flow, often associated with polluted air masses, can also contribute to surface concentrations due to entrainment. Breeze events are often challenging for meteorological and air quality simulations as the timing and strength of the breeze are key for correctly simulating pollution events (Loughner et al., 2011; 2014; Goldberg et al., 2014; Caicedo et al., 2019). To further understand these events and application to coastal environments, this study presents the evolution of two bay-breeze events and simultaneous ozone vertical profiles using the unique marine data set from the OWLETS-2 campaign in the Chesapeake Bay. Using various Doppler

wind lidar scanning techniques and derivations, the development of two distinctively different bay-breeze events were detailed in relation to surface and vertical structure of ozone.

The analysis of the wind circulation showed that the intensity of the offshore flow plays an important role in the development of the bay-breeze on both days. The two contrasting breeze days show that varying vertical motion, strength, and dilution volume play an important role in the vertical distribution of ozone and therefore is key in understanding ozone vertical structure during breeze events. The first, 29 June 2018, experienced relatively stronger offshore flow (~3 m/s) preceding the bay-breeze onset while 30 June 2018 displayed calmer offshore winds (~1 m/s). The onset of the bay-breeze was detected at ~10:00 LST on 29 June and ~07:00 LST on 30 June. An earlier onset of the bay-breeze is supported by weaker winds on the second case study day. The strength of the offshore flow was also key in the daytime development of the bay-breeze. While both days experienced an initial weakening of offshore flow to allow for the formation of the bay-breeze, 29 June offshore flow increased progressively throughout the day likely limiting the horizontal and vertical extent of the bay-breeze (up to 500 m). 30 June with weaker daytime lofted offshore flow presented a deeper bay-breeze flow (up to 800 m).

Vertical motions were observed using vertical stares (non-scanning mode) performed by the Doppler wind lidar. Enhanced vertical velocity variance during the bay-breeze was observed in the lofted offshore flow with higher values on 29 June 2018. The offshore flow will advect land-generated thermals offshore above the bay-breeze flow accounting for the enhanced vertical velocity variance observed. Upwards vertical motions were significantly enhanced on 30 June and associated with a decrease in surface ozone concentrations, and higher ozone values were found lofted above the surface near the lofted offshore flow likely indicating transport of ozone from inland sources. It was observed that high surface ozone concentrations were measured

427 during times of relatively low or decreasing BBH and weak vertical upwards motion. For 29
428 June, the highest ozone was observed during a decrease (~ 400 m to 500 m) in the BBH while 30
429 June showed the highest ozone during the early development of the bay-breeze flow (below 600
430 m) with high mixing ratios of ozone aloft (up to ~1700 m) later in the day. Although this study
431 focuses on the BBH (i.e., dilution volume) and bay-breeze dynamics which play an important
432 role in pollutant concentrations, the sources and chemistry behind the ozone concentrations
433 should not be neglected but are beyond the scope of this study. In summary, the observed
434 evolution of the bay breeze explains the vertical stratification of ozone measured by the ozone
435 lidar. On 29 June, ozone concentrations are contained within the relatively lower (or decreasing)
436 BBH displaying little vertical motions and allowing for higher surface concentrations of ozone in
437 a smaller dilution volume. The following day, 30 June, displays the highest surface ozone
438 concentration during low BBH. This day eventually develops a deeper BBH than the previous
439 day along with enhanced upwards vertical motions likely preventing pollutants from the
440 accumulating near the surface. Accordingly, enhanced lofted ozone concentrations within the
441 offshore flow are maintained above the surface. The elevated ozone concentrations within the
442 offshore flow likely contain ozone from inland sources.

443 The OWLETS-2 campaign offered high-resolution marine observations; however, future
444 campaigns should consider augmented thermodynamic profiling to better define boundary layer
445 stability. Additional turbulent parameters can aid in questions about boundary layer entrainment
446 and ultimately help in the understanding of the impact of bay-breeze events and their
447 contribution to surface pollution. Inland penetration depending on strength of bay-breeze can
448 also impact local air quality and therefore should be explored. Both dilution volume and
449 transport are an important mechanism for air quality which can be influenced by breeze

450 circulations and therefore impact coastal air quality. Better understanding of this complex
451 relationship during bay breeze and ozone vertical distribution can also aid in improving
452 simulations of local circulation and air quality events.

453

454

455 Acknowledgements

456 This study was supported in part by the Maryland Department of Environment Contract
457 (U00P9400984), and NASA Goddard Space and Flight Center under task 156 to the Joint Center
458 for Earth Systems Technology. The National Oceanic and Atmospheric Administration –
459 Cooperative Science Center for Earth System Sciences and Remote Sensing Technologies
460 (NOAA-CESSRST) under the Cooperative Agreement Grant #: NA16SEC4810008, for partial
461 support of Dr. Ruben Delgado. The NASA LaRC authors gratefully acknowledge the help of
462 William Carrion and Joseph Sparrow in the set-up and operation of the ozone lidar at Hart-Miller
463 Island.
464

References

Abdi-Oskouei, M., Carmichael, G., Christiansen, M., Ferrada, G., Roozitalab, B., Sobhani, N., Wade, K., Czarnetzki, A., Pierce, R. B., Wagner, T., Stanier, C. (2020). Sensitivity of Meteorological Skill to Selection of WRF-Chem Physical Parameterizations and Impact on Ozone Prediction During the Lake Michigan Ozone Study (LMOS), Journal of Geophysical Research-Atmospheres, 125(5).

Azorin-Molina C., Connell B. H., and Baena-Calatrava R. (2009). Sea-breeze convergence zones from AVHRR over the Iberian Mediterranean area and the Isle of Mallorca, Spain. J Appl Meteorol Climatol 48:2069–2085

Banta, R. M., Olivier, L. D., and Levinson, D. H. (1993). Evolution of the Monterey Bay sea-breeze layer as observed by pulsed Doppler lidar. J. Atmos. Sci., 50, 3959–3982

Banta, R. M., Senff, C. J., Nielsen-Gammon, J., Darby, L. S., Ryerson, T. B., Alvarez, R. J., Sandberg, S. P., Williams, E. J., and Trainer, M. (2005). A Bad Air Day in Houston. Bull. Am. Meteorol. Soc., 86(5), 657–669, doi.org/10.1175/BAMS-86-5-657

Barlow, J. F., Dunbar, T. M., Nemitz, E. G., Wood, C. R., Gallagher, M. W., Davies, F., O'Connor, E., and Harrison, R. M. (2011). Boundary layer dynamics over London, UK, as observed using Doppler lidar during REPARTEE-II. Atmos. Chem. Phys., 11, 2111–2125, https://doi.org/10.5194/acp-11-2111-2011.

Bonin, T. A., Carroll, B. J., Hardesty, R. M., Brewer, W. A., Hajny, K., Salmon, O. E., and Shepson, P. B. (2018). Doppler lidar observations of the mixing height in Indianapolis using an automated composite fuzzy logic approach. Journal of Atmospheric and Oceanic Technology,35(3), 473–490. htt ps://doi.org/10.1175/JTECH-D-17-0159.1

Caicedo, V., Rappenglueck, B., Cuchiara, G., Flynn, J., Ferrare, R., Scarino, A. J., Berkoff, T., Senff, C., Langford, A., and Lefer, B. (2019). Bay-breeze and sea breeze circulation impacts on the planetary boundary layer and air quality from an observed and modeled DISCOVER-AQ Texas case study. Journal of Geophysical Research: Atmospheres, 124, 7359– 7378. doi.org/10.1029/2019JD030523

Conley, S. A., Faloona, I. C., Lenschow, D. H., Karion, A., and Sweeney, C. (2014). A low-cost system for measuring horizontal winds from single-engine aircraft. Journal of Atmospheric and Oceanic Technology, 31, 1312–1320, doi:10.1175/JTECH-D-13-00143.1.

Curry M., Hanesiak J., Kehler S., Sills D. M. L., and Taylor N. M. (2017). Ground-based observations of the thermodynamic and kinematic properties of lake-breeze fronts in southern Manitoba, Canada. Boundary-Layer Meteorol 163:143–159.

Dacic, N., Sullivan, J. T., Knowland, K. E., Wolfe, G. M., Oman, L. D., Berkof, T. A., Gronoff, G. P., (2020). Evaluation of NASA's high-resolution global composition simulations: Understanding a pollution event in the Chesapeake Bay during the summer 2017 OWLETS campaign, Atmospheric Environment, 22.

Darby, L. S. (2005). Cluster Analysis of Surface Winds in Houston, Texas, and the Impact of Wind Patterns on Ozone. J. Appl. Meteorol., 44(12), 1788–1806, doi.org/10.1175/JAM2320.1

Darby, L.S., McKeen, S.A., Senff, C.J., White, A.B., Banta, R.M., Post, M.J., Brewer, W.A., Marchbanks, R., Alvarez II, R.J., Peckham, S.E., Mao, H., and Talbot, R. (2007). Ozone differences between near-coastal and offshore sites in New England: Role of meteorology. J. Geophys. Res. 112, D16S91. doi:10.1029/ 2007JD008446

510 Darby L. S., Banta R. M., and Pielke R. A. (2002). Comparisons between mesoscale model
511 terrain sensitivity studies and doppler lidar measurements of the sea breeze at Monterey
512 Bay. Mon Weather Rev 12:2813–2838
513 De Young, R., Carrion, W., Ganoe, R., Pliutau, D., Gronoff, G., Berkoff, T., and Kuang, S.
514 (2017). Langley mobile ozone lidar: Ozone and aerosol atmospheric profiling for air
515 quality research. Appl. Opt., 56, 721–730, https://doi.org/10.1364/AO.56.000721.
516 Farris, B. M., Gronoff, G. P., Carrion, W., Knepp, T., Pippin, M., and Berkoff, T. A. (2018).
517 Demonstration of an off-axis parabolic receiver for near-range retrieval of lidar ozone
518 profiles. Atmos. Meas. Tech. Discuss., https://doi.org/10.5194/amt-2018-178.
519 Goldberg, D. L., Loughner, C. P., Tzortziou, M., Stehr, J. W., Pickering, K. E., Marufu, L. T.,
520 and Dickerson, R. R. (2014). Higher surface ozone concentrations over the Chesapeake
521 Bay than over the adjacent land: observations and models from the DISCOVER-AQ and
522 CBODAQ campaigns. Atmos. Environ. 84, 9e19.
523 http://dx.doi.org/10.1016/j.atmosenv.2013.11.008.
524 Gronoff G., Robinson J., Berkoff T., Swap R., Farris B., Schroeder J., Halliday H., Knepp T.,
525 Spinei E., Carrion W., Adcock E., Johns Z., Allen D., Pippin M. (2019). A method for
526 quantifying near range point source induced O3 titration events using Co-located Lidar
527 and Pandora measurements. Atm. Env., 204, 43-52, ISSN 1352-2310,
528 https://doi.org/10.1016/j.atmosenv.2019.01.052.
529 Heffter J. L. (1980). Transport Layer Depth Calculations. Second Joint Conference on
530 Applications of Air Pollution Meteorology, New Orleans, Louisiana.
531 Hogan, R. J., Grant, A. L. M., Illingworth, A. J., Pearson, G. N., and O'Connor, E. J. (2009).
532 Vertical velocity variance and skewness in clear and cloud-topped boundary layers as

533 revealed by Doppler lidar. Quart. J. Roy. Meteor. Soc., 135, 635–643,
534 https://doi.org/10.1002/qj.413.
535 King P. W. S., Leduc M. J., Sills D. M. L., Donaldson N. R., Hudak D, R., Joe P, Murphy P. B.
536 (2003). Lake breezes in southern Ontario and their relation to tornado climatology.
537 Weather Forecast 18:795–807
538 Kingsmill, D. E. (1995). Convection initiation associated with a sea-breeze front, a gust front and
539 their collision. Mon. Wea. Rev., 123, 2913-2933
540 Leblanc, T., Sica, R. J., van Gijsel, J. A. E., Godin-Beekmann, S., Haefele, A., Trickl, T., Payen,
541 G., Liberti, G. (2016). Proposed standardized definitions for vertical resolution and
542 uncertainty in the ndacc lidar ozone and temperature algorithms–part 2: ozone dial
543 uncertainty budget. Atmos. Meas. Tech. 9 (8), 4051–4078.https://www.atmos-meas-
544 tech.net/9/4051/2016/.
545 Leblanc,T., Brewer, M. A., Wang, P. S., Granados-Muñoz, M. J., Strawbridge, K. B., Travis, M.,
546 Firanski, B., Sullivan, J. T., McGee, T. J., Sumnicht, G. K., Twigg, L. W., Berkoff, T. A.,
547 Carrion, W., Gronoff, G., Aknan, A., Chen, G., Alvarez, R. J., Langford, A.O., Senff, C.
548 J., Kirgis, G., Johnson, M. S., Kuang, S., Newchurch, M. J. (2018).Validation of the
549 TOLNet lidars: the southern California ozone observation Project(SCOOP). Atmos.
550 Meas. Tech. 11, 6137–6162.
551 Loughner, C. P., Allen, D. J., Pickering, K. E., Dickerson, R. R., Zhang, D.-L., and Shou, Y. X.
552 (2011). Impact of fair-weather cumulus clouds and the Chesapeake Bay-breeze on
553 pollutant transport and transformation. Atmos. Environ., 45, 4060–4072.
554 Loughner C. P., Tzortziou, M., Follette-Cook, M., Pickering, K. E., Goldberg, D., Satam, C.,
555 Weinheimer, A., Crawford, J. H., Knapp, D. J., Montzka, D. D., and Diskin, G. S. (2014).

556 Impact of bay-breeze circulations on surface air quality and boundary layer export. J.
557 Appl. Meteorol. Climatol. 53(7): 1697–713. doi:10.1175/JAMC-D-13-0323.1
558 Mariani, Z., Dehghan, A., Joe, P. ,and Sills, D. M. (2018). Observations of lake breeze events
559 during the Toronto 2015 Pan-American Games. Bound.-Layer Meteor., 166, 113–135,
560 https://doi.org/10.1007/s10546-017-0289-3.
561 Mazzuca, G. M., Pickering, K. E., New, D. A., Dreessen, J., Dickerson, R. R. (2019). Impact of
562 bay breeze and thunderstorm circulations on surface ozone at a site along the Chesapeake
563 Bay 2011–2016, Atmospheric Environment, 198, 351-365,
564 https://doi.org/10.1016/j.atmosenv.2018.10.068
565 Pearce R.P. (1955) The calculation of a sea-breeze circulation in terms of the differential heating
566 across the coastline. Q J R Meteorol Soc 81:351–381
567 Philandras C. M., Metaxas, D. A., Nastos P, T. (1999). Climate variability and urbanization in
568 Athens. Theoretical and Applied Climatology63: 65–72
569 Ren, X., Salmon, O. E., Hansford, J. R., Ahn, D., Hall, D., Benish, S. E., Stratton, P. R., He, H., Sahu, S.,
570 Grimm, C., Heimburger, A. M. F., Cohen, M. D., Stunder, B., Salawitch, R. R., Ehrman, S. H.,
571 Shepson, P. B., and Dickerson, R. R (2018). Methane emissions from the Baltimore-Washington
572 area based on airborne observations: Comparison to emissions inventories, *J. Geophys. Res. –*
573 *Atmos.*, 123, 8869–8882, doi: 10.1029/2018JD028851.
574 Sills, D., Taylor, P., King, P., Hocking, W., and Nichols, I. (2002). ELBOW 2001—Studying the
575 relationship between lake breezes and severe weather: Project overview and preliminary
576 results. Preprints, 21th Conf. on Severe Local Storms, San Antonio, TX, Amer. Meteor.
577 Soc., 611–614

578 Sills, D. M. L., Brook, J. R., Levy, I., Makar, P. A., Zhang, J., Taylor, P.A. (2011). Lake breezes
579 in the southern Great Lakes region and their influence during BAQS-Met 2007. Atmos
580 Chem Phys 11:7955–7973
581 Snyder, B. J. and Strawbridge, K. B. (2004). Meteorological summary of the Pacific 2001 air
582 quality field study. Atmospheric Environment, this issue,
583 doi:10.1016/j.atmosenv.2004.02.058
584 Stauffer R. M. and Thompson, A. M. (2015). Bay breeze climatology at two sites along the
585 Chesapeake bay from 1986–2010: Implications for surface ozone, J Atmos Chem,
586 72:355–372, doi: 10.1007/s10874-013-9260-y
587 Sullivan, J. T., Timothy, B., Guillaume, G., Travis, K., Margaret, P., Danette, A., Laurence, T.,
588 Berkoff, T., Gronoff, G., Knepp, T., Pippin, M., Allen, D., Twigg, L., Swap, R.,
589 Tzortziou, M., Thompson, A. M., Stauffer, R. M., Wolfe, G. M., Flynn, J., Pusede, S. E.,
590 Judd, L. M., Moore, W., Baker, B. D., Al-Saadi, J., McGee, T. J. (2019). The ozone
591 water-land environmental transition study: an innovative strategy for understanding
592 Chesapeake Bay pollution events. Bull. Am. Meteorol. Soc. 100, 291–306.
593 Tijm, A. B. C., Holtslag, A. A. M., and van Delden, A. J. (1999). Observations and Modeling of
594 the Sea Breeze with the Return Current. Monthly Weather Review, 127(5), 625–640,
595 doi.org/10.1175/1520-0493(1999)127<0625:OAMOTS>2.0.CO;2
596 Tucker, S. C., Brewer, W. A., Banta, R. M., Senff, C. J., Sandberg, S. P., Law, D. C.,
597 Weickmann, A. M., and Hardesty, R. M. (2009). Doppler lidar estimation of mixing
598 height using turbulence, shear, and aerosol profiles. J. Atmos. Oceanic Technol., 26, 673–
599 688, https://doi.org/10.1175/2008JTECHA1157.1.

Van der Molen, M. K., Dolman, A. J., Waterloo, M. J. and Bruijnzeel, L. A. (2006). Climate is affected more by maritime than by continental land use change: A multiple scale analysis. Global and Planetary Change, 54, 128–149.

Vemado, F. and Pereira Filho, A. J. (2016). Severe weather caused by heat island and sea breeze effects in the metropolitan area of Sao Paulo, Brazil. Adv. Meteorol. 2016,1–13.

Vermeuel, M. P., Novak, G. A., Alwe, H. D., Hughes, D. D., Kaleel, R., Dickens, A. F., Kenski, D., Czarnetzki, A. C, Stone, E. A., Stanier, C. O., Pierce, R. B., Millet, D. B., Bertram, T. H., (2019). Sensitivity of Ozone Production to NOx and VOC Along the Lake Michigan Coastline, Journal of Geophysical Research-Atmospheres, 124(20), 10989-11006.

Zhang, D. L., Shou, Y. X., and Dickerson, R. R., (2009). Upstream urbanization exacerbates urban heat island effects, Geophysical Research Letters, 36.

Zhang, D. L., Shou, Y. X., Dickerson, R. R., and Chen, F., (2011). Impact of Upstream Urbanization on the Urban Heat Island Effects along the Washington-Baltimore Corridor, Journal of Applied Meteorology and Climatology, 50(10), 2012-2029.